Acoustofluidics along inclined surfaces based on AlN/Si Rayleigh surface acoustic waves

Yong Wang[a,c], Xiang Tao[b,c], Ran Tao[c], Jian Zhou[d], Qian Zhang[a], Dongyang Chen[a], Hao Jin[b], Shurong Dong[b], Jin Xie[a,*], and Yong Qing Fu[c,*]

[a] The State Key Laboratory of Fluid Power and Mechatronic Systems, Zhejiang University, Hangzhou 310027, China

[b] College of Information Science and Electronic Engineering, Zhejiang University, Hangzhou 310027, China

[c] Faculty of Engineering and Environment, University of Northumbria, Newcastle upon Tyne NE1 8ST, UK

[d] State Key Laboratory of Advanced Design and Manufacturing for Vehicle Body, College of Mechanical and Vehicle Engineering, Hunan University, Changsha 410082, China

* Corresponding authors: E-mail: xiejin@zju.edu.cn; Richard.fu@northumbria.ac.uk

ABSTRACT

Conventional acoustofluidics are restricted to manipulation of droplets on a flat surface, and there is an increasing demand for acoustofluidic devices to be performed at inclined surfaces to facilitate multilayered microfluidic device design and enhance system compactness. This paper reports theoretical and experimental studies of acoustofluidic behaviors (including transportation/pumping and jetting) along inclined surfaces using AlN/Si Rayleigh surface acoustic waves (SAWs). It has been demonstrated that for droplets with volume smaller than 3 μL, they could be efficiently transported on arbitrary inclined surfaces. The gravity effect would play a more and more important role in uphill climbing with the increased inclination angle. When the inclination angle was increased up to 90º, a higher threshold power was needed to transport the droplet and the maximum droplet volume which can be pumped also reached its minimum value. Effects of surface inclination angle on droplet jetting angles could be neglected for their volumes less than 2 μL. Moreover, microfluidic and acoustic heating performances of AlN/Si SAWs were further studied and compared with those conventional ZnO/Si SAWs with the same electrode configurations.

Keywords: Acoustofluidics, Inclined surfaces, AlN film, Surface acoustic waves

1. Introduction

Surface acoustic wave (SAW) devices have attracted great attention for microfluidic and lab-on-a-chip applications due to their low cost, simple fabrication process, fast response and high precision [1-4]. Various microfluidic functions, including streaming [5, 6], mixing [7, 8], concentration [9], pumping [10], splitting [11], jetting [12, 13], nebulization [14-16] and particle/cell manipulation and separation [17, 18] have been demonstrated using SAW techniques. Conventional SAW devices for acoustofluidics are mostly made on bulk $LiNbO_3$ substrates on account of their large electromechanical coupling coefficients (5~11%) and resulting in low threshold powers [12, 19]. However, these bulk piezoelectric substrates are often expensive, less easily integrated with electronics for signal processing and easily broken at a high power due to the brittle nature of the ceramic material under a large thermal/electrical shock [20-22].

SAW technologies based on piezoelectric thin films such as ZnO and AlN present several distinct advantages over bulk substrates, including flexible electrode designs, high breakdown voltage and easily integrated with other electronics [4, 23]. Another key advantage using piezoelectric thin films is that they can be easily deposited onto different substrates such as silicon, glass, metal and polymer with new functions, and then different acoustic velocities or wave modes can be obtained [24-27]. Therefore, thin film SAW techniques have been considered as one of the key directions for acoustofluidics and lab-on-a-chip applications. In recent years, many acoustofluidic devices based on ZnO film SAWs

have been reported [28-30]. However, ZnO films are generally considered to be unstable in liquid environment with weak mechanical and corrosion properties, thus are less ideal for acoustofluidics [31]. Besides, as Zn is considered as a contaminant in the complementary metal oxide semiconductor (CMOS) processes, ZnO film SAW processing technologies are also considered to be incompatible with CMOS processes.

In comparison with ZnO films, AlN films have better chemical/thermal stability, higher acoustic velocity, higher breakdown voltage, and are also compatible with CMOS processes [32, 33]. Therefore, AlN film SAWs have great potentials for both sensing and acoustofluidic applications. At present, many studies using AlN film SAWs for sensing applications have been reported [34-36], whereas acoustofluidics based on AlN film SAWs have seldomly been reported [20, 21]. Moreover, most acoustofluidic devices are restricted to manipulation of droplets on a flat or inverted surface [37]. However, transportation of droplets along inclined surfaces can facilitate realization of designs for wearable, flexible multilayered or three-dimensional (3D) microfluidic devices, thereby enhancing structure compactness and volumetric capacity. Recently, droplet manipulations on inclined surfaces have been demonstrated using electrowetting, electrostatic actuation and mechanowetting on transverse waves [38-41]. However, the uphill actuation of the droplet along inclined surfaces using the SAWs has not been reported yet as far as we have searched. In this paper, we investigated acoustofluidic behaviors (including transportation/pumping and jetting) along the flat and inclined surfaces using AlN/Si Rayleigh surface acoustic waves. Moreover, we also fabricated a ZnO/Si SAW device with the same electrode configurations (wavelength, aperture and finger pairs) as those of AlN/Si SAWs and compared their microfluidic and acoustic heating performances.

2. Theoretical analysis

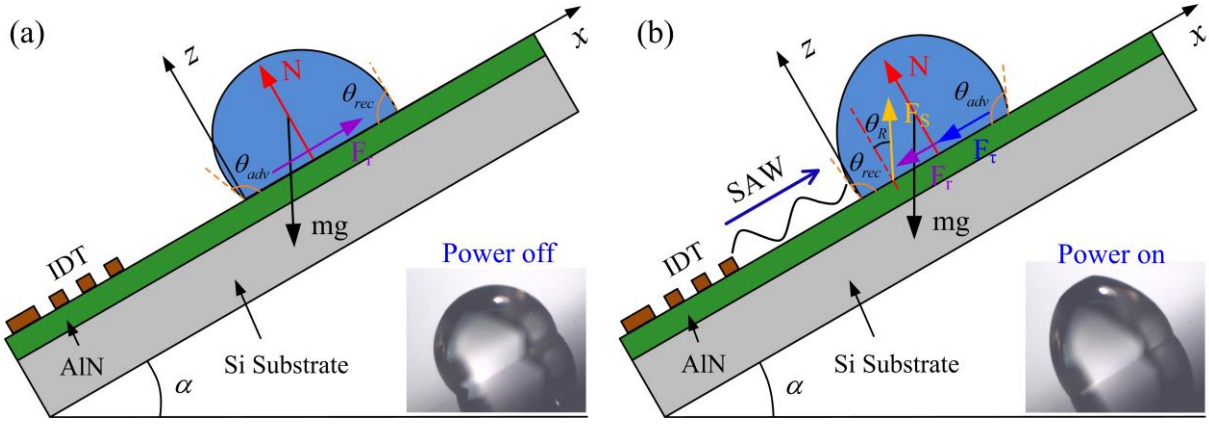

Fig. 1. The droplet force analysis on the inclined surface (a) without and (b) with agitation of the SAW.

Fig. 1 shows the droplet force analysis on the inclined surface without and with agitation of the SAW. In the absence of SAW, the force balance of the droplet is mainly governed by three forces: (i) the gravitational force *mg* which is intended to deform the droplet; (ii) the hysteresis resistance force F_r due to contact angle hysteresis (CAH) which is attempted to prevent the motion; and (iii) the normal reaction force *N* from the substrate [42]. Thus, the surface needs to exhibit a large CAH to hold the droplet on the inclined surface at a static equilibrium. Moreover, there is also a critical value for surface inclination angles, above which, the droplet begins to move. The surface inclination angle at which the droplet is at the point of impending motion is defined as the critical inclination angle α_S [43, 44]. Then the force balance of the sessile droplet on the inclined surface in the *x*-axis direction without SAW agitation can be given by

$$\begin{cases} F_r = mg\sin\alpha & \text{for } \alpha < \alpha_S \\ F_r = k\gamma L(\cos\theta_{rec} - \cos\theta_{adv}) & \text{for } \alpha = \alpha_S \end{cases} \quad (1)$$

where *m* is the mass of the droplet, *g* is the acceleration of the gravity, α is the surface inclination angle, *k* is a dimensionless constant, γ is the liquid-vapor interfacial tension, *L* is a length scale related to the droplet, θ_{adv} and θ_{rec} are the advancing and receding angles, respectively.

When a droplet is put on the surface of the propagating wave, the energy of Rayleigh wave will be dissipated into the droplet, generating an acoustic streaming force and inducing the droplet inertial streaming, known as acoustic streaming [45, 46]. Once the droplet starts moving, a shear force is generated due to the rate of fluid strain formed along the contact line between the droplet and hydrophobic surface [47]. Therefore, there are five main forces applied onto the droplet on the inclined surface, namely, the SAW streaming force F_S, the shear force F_τ, the droplet gravitational force mg, the hysteresis resistance force F_r and the reaction force N from the substrate, as shown in Fig. 1(b).

The SAW streaming force is a body force, which can be written as [46]

$$F_S = -\rho_f (1+\alpha_1^2)^{3/2} A^2 w^2 k_i \exp 2(k_i x + \alpha_1 k_i z) \tag{2}$$

where ρ_f is the liquid density, A is the SAW amplitude, w is the angular frequency, k_i is the imaginary part of the leaky SAW wave number and refers to effective radiation of SAW energy into the droplet. Here, α_1 = -jα, α represents the attenuation constant, $\alpha^2 = 1 - (v_l/v_f)^2$, where v_l and v_f are the leaky SAW velocity and sound velocity in the liquid respectively. The direction of SAW streaming force is along the Rayleigh angle θ_R, which can be expressed as

$$\theta_R = \sin^{-1}(v_f / v_s) \tag{3}$$

where v_f is the sound velocity in the liquid, and v_s is the SAW phase velocity in the substrate.

The shear force F_τ due to the rate of fluid strain formed along the contact line can be given by

$$F_\tau = A_w \left(\mu \frac{dV}{dy} \right) \tag{4}$$

where A_w is the droplet contact area, μ is the droplet fluid viscosity, V is the fluid velocity, and y is the distance normal to the contact surface.

The resistance force caused by the contact angle hysteresis during the droplet movement can be written as [48]

$$F_r = k\gamma L(\cos\theta_{rec} - \cos\theta_{adv}) \tag{5}$$

The force balance of the droplet in the x-axis direction during the pumping process can be derived as

$$F_S \sin\theta_R - F_r - F_\tau - mg\sin\alpha = ma_x \tag{6}$$

From Eq. (6), we can see that the droplet motion along the inclined surface can be affected by the SAW streaming force, the hysteresis resistance force, the droplet gravity and the surface inclination angle. As the input power is increased, the SAW streaming force applied onto the droplet increases, resulting in the increase of the droplet motion speed. As the inclination angle is increased (α < 90°), the gravity component along the inclined surface increases, thus causing the decrease of droplet motion speed.

3. Experimental

AlN films of ~4.8 μm thickness were deposited onto 4-inch silicon (100) substrates using DC magnetron sputtering process. The details of the film deposition process have been described in the previous work [20, 21]. The crystal orientation of AlN films was analyzed using X-ray diffraction (XRD, D5000, Siemens) with Cu-K_α radiation (λ = 1.5406 Å). The cross-sectional microstructures of the AlN films were characterized using a scanning electron microscope (SEM, Hitachi SU70, Japan). Then the SAW devices were fabricated on AlN/Si substrates by patterning a 100 nm thickness Cr/Au film to form the IDT electrodes. Each IDT was composed of 40 pairs of fingers, with a spatial periodicity of 64 μm and an acoustic aperture of 4.9 mm. The responses of the SAW device were measured using an RF network analyzer (Agilent E5071C).

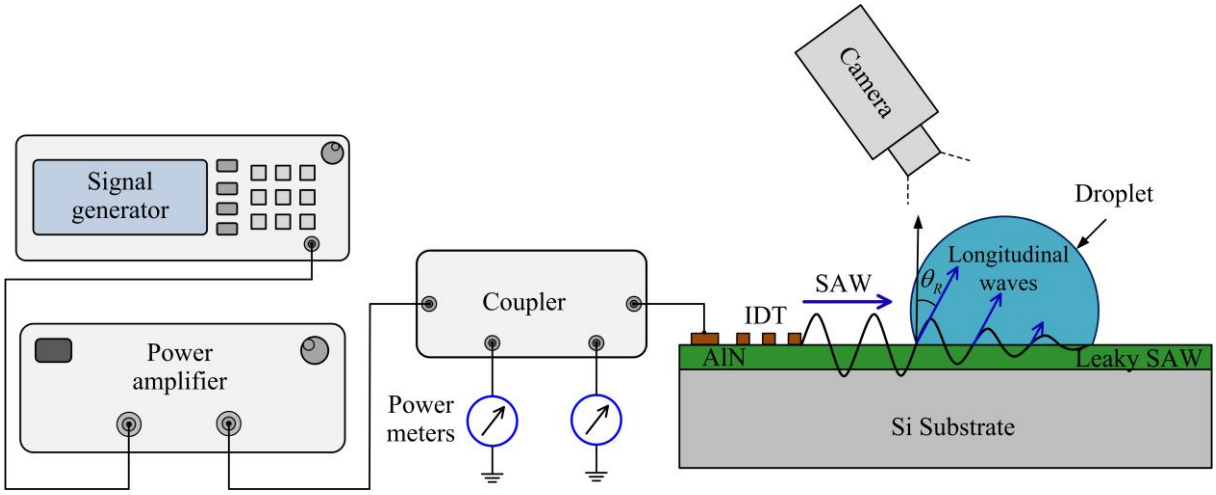

Fig. 2. The schematic of experimental setup for microfluidic tests.

Surface of the SAW device was coated with a layer of ~300 nm thick CYTOP (Asahi Glass Co., Tokyo, Japan) to make the surface hydrophobic. A drop shape analyzer (Kruss DSA30S) was used to characterize the hysteresis resistance force of the droplet motion through measuring the droplet advancing and receding angles. After the surface hydrophobic treatment, the droplet contact angle was increased from 79.6° to 104.3° and the contact angle hysteresis ($\Delta\theta = \theta_{adv} - \theta_{rec}$) was decreased from 59.6° to 11.2°. For microfluidic and acoustic heating tests, the SAW devices were placed on an aluminum alloy holder to increase the heat dissipation. The RF signal was generated using a signal generator (Marconi 2024, Plainview, USA) and amplified by a power amplifier (Amplifier research, 75A250, Souderton, USA). The amplified signal was then connected to a coupler before being fed into the SAW device, as shown in Fig. 2. The incident and reflected powers of the SAW device were measured using two power meters connected to the coupler. Finally, the real input SAW power was determined by the power difference between two power meters. The acoustofluidic behaviors were recorded using a standard video camera. For SAW heating tests, the device temperature was measured using an infrared video camera (ThermaCAM^{TM} SC640), which has been calibrated according to the emissivity of object.

4. Results and discussion

4.1. Film and device characterization

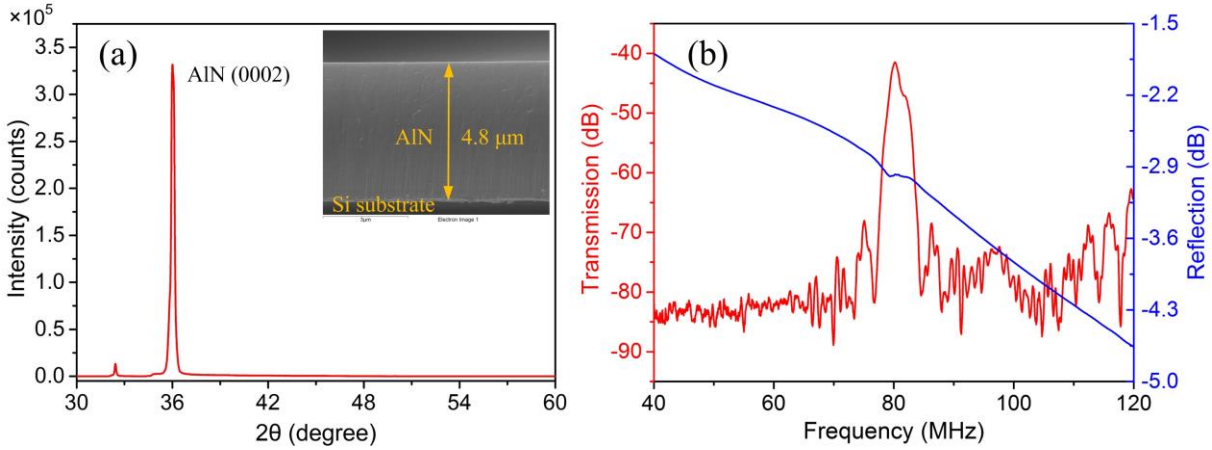

Fig. 3. (a) XRD pattern and SEM cross-sectional microstructure of AlN films and (b) signal characterization of AlN/Si SAW device.

Fig. 3(a) shows the characterization of AlN films. XRD results show that AlN films have a good c-axis (0002) crystal orientation with the diffraction angle 2θ of ~36°. SEM cross-section images of the AlN films reveal that the films have

vertical columnar grains on the silicon substrate and the thickness of AlN films is about 4.8 μm. The frequency response of the SAW device is shown in Fig. 3(b). The device exhibits a resonant peak at the frequency of 80.35 MHz, corresponding to the fundamental Rayleigh wave mode with a calculated wave velocity of about 5142.4 m/s. Moreover, the transmission band at the resonance has a strong out-of-band rejection of ~40 dB, indicating a good performance of the SAW device.

4.2. Acoustofluidics along the inclined surfaces

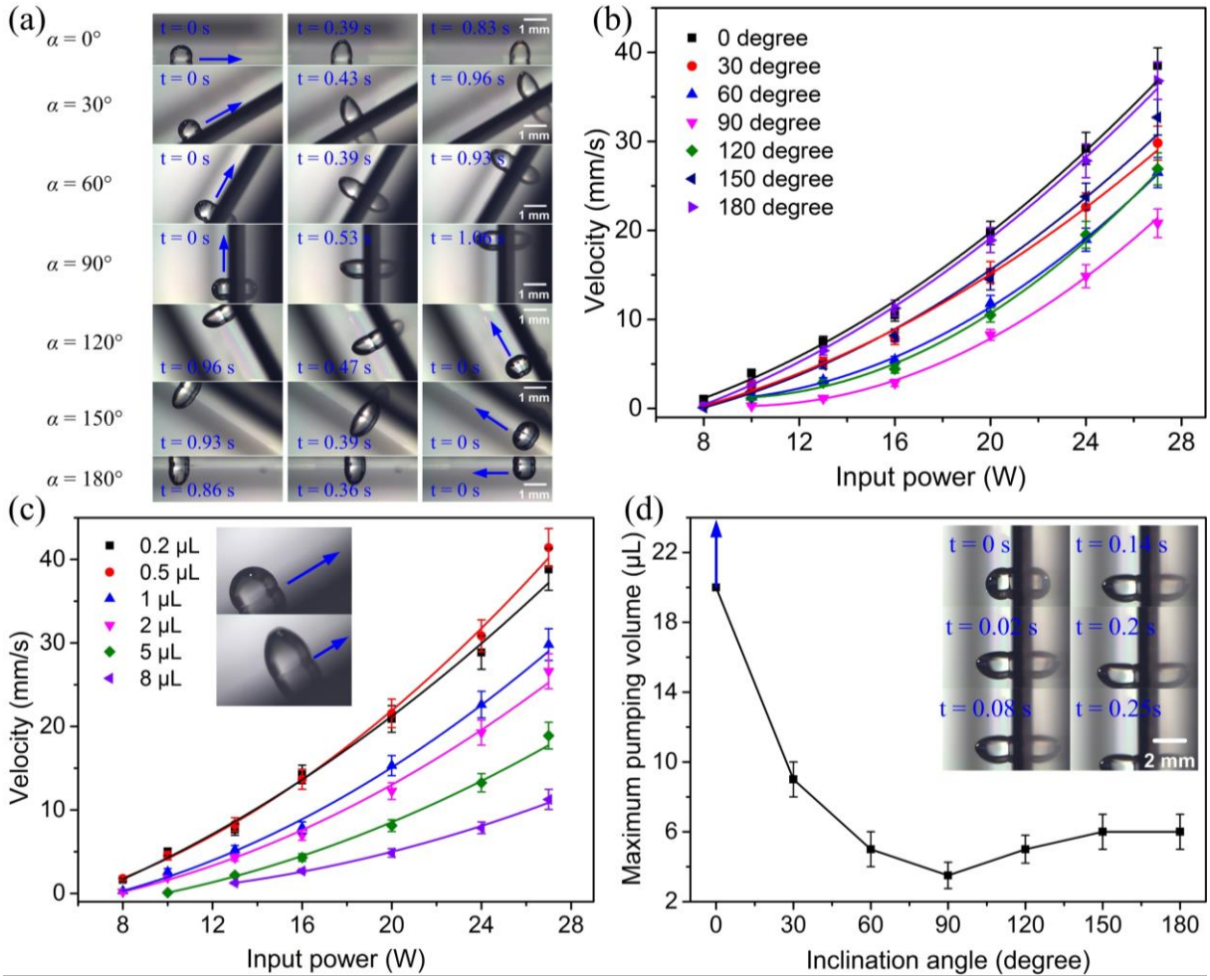

Fig. 4. (a) Water droplet (1 μL) pumping images along inclined surfaces with an input SAW power of 12 W, (b) droplet average pumping velocities along different inclination angles under different input SAW powers, (c) pumping velocities of the droplets with different volumes on 30° inclined surface under different input SAW powers, and (d) the maximum droplet pumping volume under different inclination angles, the insert shows the pumping images of the 3 μL droplet.

Fig. 4(a) shows droplet transportation/pumping images along inclined surfaces. When the droplet has a volume smaller than 3 μL, they can be pumped on arbitrary inclined surfaces. Fig. 4(b) shows the average pumping velocities of the droplet on different inclination angles under different input SAW powers. Results show that the pumping velocity is increased with the input SAW power when the inclination angle is fixed. At the same input SAW power, the droplet pumping velocity is decreased with the inclination angle increased from 0° to 90°, and reaches the minimum value at 90° inclination angle. As the inclination angle is further increased from 90° to 180°, the droplet pumping velocity is increased. The results are in good agreement with the theoretical analysis in Eq. (6).

Fig. 4(c) shows droplet volume effects on the pumping velocity at 30° inclination angle. The pumping velocity is decreased with the droplet volumes increased from 0.5 μL to 8 μL at a constant input power. The components of the droplet

gravity along the inclined surface per unit area are estimated to be 4.4, 4.9, 5.2, 5.6, 6, 6.2 μN/mm^2 for the droplets with volumes of 0.2, 0.5, 1, 2, 5, 8 μL, respectively. Therefore, the SAW streaming force per unit area applied onto smaller droplet exhibits a steeper slope for the curve of the pumping velocity [14]. In addition, the pumping velocity of the 0.2 μL droplet is slightly lower than that of 0.5 μL droplet, probably due to surface microstructure of the CYTOP layer, which causes a decreased contact angle and increased hysteresis resistance force at the volume of 0.2 μL [49].

Fig. 4(d) shows the maximum droplet volume which can be pumped under different inclination angles. When the droplet was pumped on a flat surface, the maximum pumping volume was above 40 μL. As the inclination angle was increased from 0° to 90°, the maximum pumping volume was decreased and reached the minimum value at 90° inclination angle. As shown in the insert of Fig. 4(d), for the droplet with volume above 3 μL, when it was pumped up on the vertical surface, the droplet would slide down from the surface. There was also a critical droplet volume on the inclined surface, above which, the droplet began to slide down. As the inclination angle was further increased from 90° to 150°, the maximum pumping volume was increased. When the droplet was pumped on an inverted surface, the adhesive force between the surface and the droplet might play a dominant role because the droplet would drop down when it has a larger volume [37].

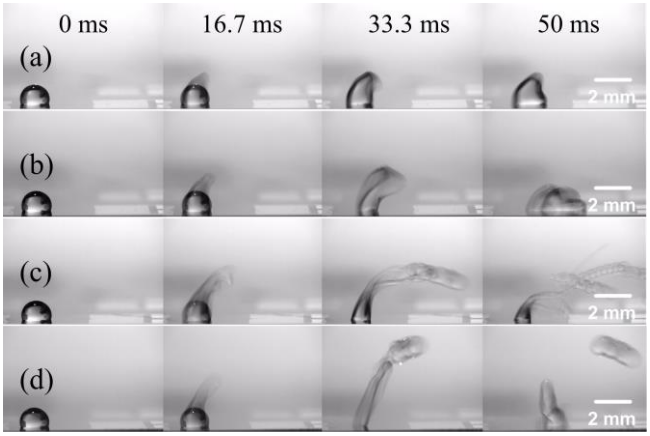

Fig. 5. Droplet (2 μL) pumping and jetting images driven by propagating waves (from left to right) under different input SAW powers (a) 27 W, (b) 32 W, (c) 38 W, (d) 44 W.

When the input SAW power was increased to dozens of watts, the water droplet began to jump rather than move on the surface, as shown in Fig. 5(b). At an input power of 32 W, due to lesser SAW energy dissipating into the droplet, the droplet could only be lifted up to a few millimeters before it dropped down to the device surface. With the further increased input SAW powers to 38 W and 44 W, much more SAW energy was dissipated into the droplet, resulting in liquid beam formation and ejection from the device surface, as shown in Fig. 5(c) and (d).

Fig. 6 shows jetting images for different volume droplets driven by the propagating waves at an input power of 44 W. When the droplet has a size smaller than 1 μL, if a higher RF power was applied to the IDTs, the droplet would break up into small droplets with size in the range of a few fL to pL, and then were lifted up from the device surface, as shown in Fig. 6(a-c). When the droplet has a larger size (above 2 μL), the jetting shape of the droplet tended to form a cylindrical liquid beam, as shown in Fig. 6(d-f). Besides, as the droplet volume was increased, the liquid at the front of ejected beam was bent down due to the gravity effect. Moreover, the maximum jetting angles are varied around 72.4° for droplets with volumes ranging from 0.2 to 10 μL. The complementary angles of the jetting angles are close to the Rayleigh angle of the AlN/Si SAW device, which can be calculated using Snell's law and is about 17°.

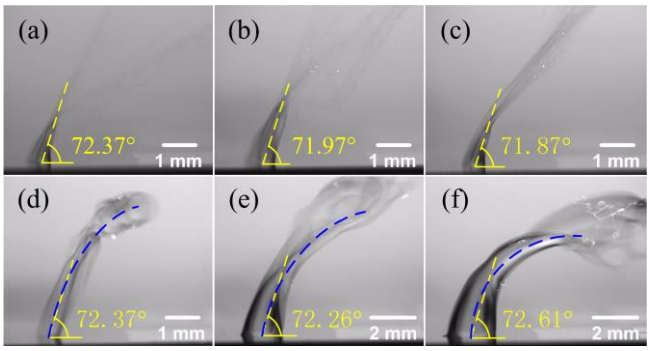

Fig. 6. Jetting images of water droplets with different volumes (a) 0.2 μL, (b) 0.5 μL, (c) 1 μL, (d) 2 μL, (e) 5 μL and (f) 10 μL, driven by propagating waves with an input SAW power of 44 W.

The propagating wave jetting of the droplet (1 μL) on the inclined surfaces with inclination angles from 0° to 180° was also investigated, and the results are shown in Fig. 7. The maximum jetting angles of the droplet under different inclination angles are varied slightly around 72.5°, following the Rayleigh angle of the AlN/Si SAW device. Therefore, when the droplet has a smaller size, the influences of surface inclination angle on the droplet propagating wave jetting angles are negligible.

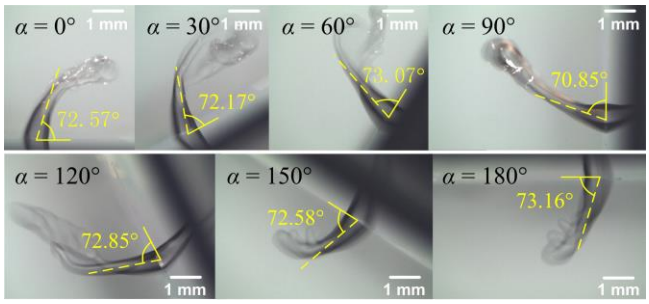

Fig. 7. Water droplet jetting images along inclined surfaces driven by propagating waves with an input SAW power of 38 W.

For standing wave jetting, a power divider was connected to the output of the coupler to generate two same RF signals. Hence, the real power for each of the IDT is half of the total input SAW power. Fig. 8(a) shows high-speed jetting images of the 5μL water droplet excited by standing waves under different input SAW powers. Results show that when a lower RF total power (below 48 W) was applied to the SAW device, the droplet was difficult to eject from the device surface and only the significant vibration and jumping of the droplet were observed. When a higher RF total power (above 60 W) was applied to the SAW device, the cylindrical liquid beam was formed and ejected vertically from the device surface. Fig. 8(b) shows the captured jetting images of water droplets with different volumes under different input SAW powers, and the results reveal that the larger the droplet volume, the more difficult the ejection of the droplet. Moreover, the maximum jetting height of the droplet was increased with the input SAW power or decreased droplet volume, as shown in Fig. 8(c).

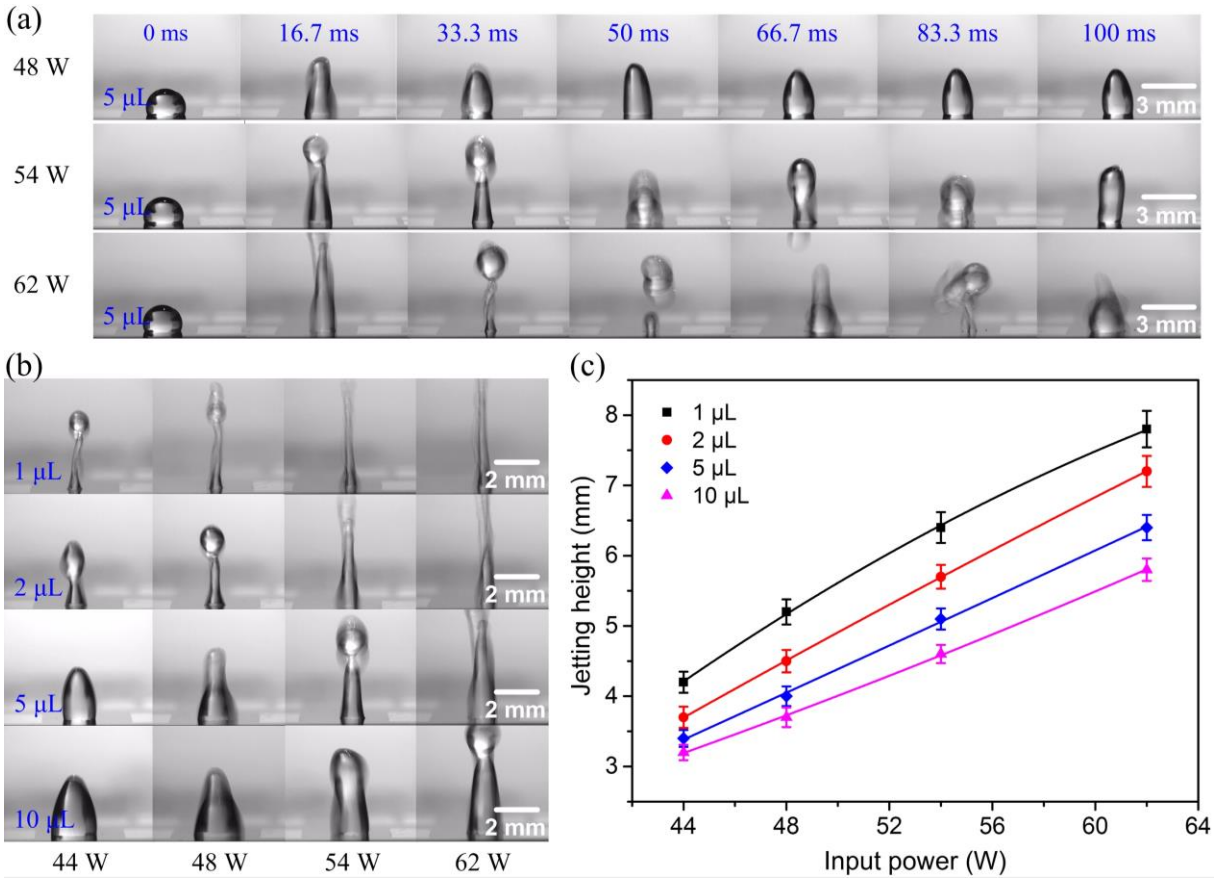

Fig. 8. (a) High-speed jetting images of the 5 μL water droplet excited by standing waves at input powers of 48W, 54 W and 62 W, (b) the captured jetting images for different volume droplets under different input SAW powers, and (c) the maximum jetting height for different volume droplets under different input SAW powers.

We also investigated the droplet jetting along inclined surfaces with inclination angles from 0° to 90° agitated using standing waves, as shown in Fig. 9. After an RF power of 54 W was applied to both IDTs of the SAW device, the acoustic streaming forces from two sides pushed the droplet upwards, forming a vertical cylindrical liquid beam and consequently the liquid beam was ejected from the device surface. For 1 μL droplet, the jetting angles under different inclination angles were nearly vertical to the device surface. The jetting angles of the 2 μL droplet on the flat and inclined surfaces were also perpendicular to the device surface, but the liquid beam on the inclined surface was tended to bend downwards at the tip of the elongated beam due to the gravity effect.

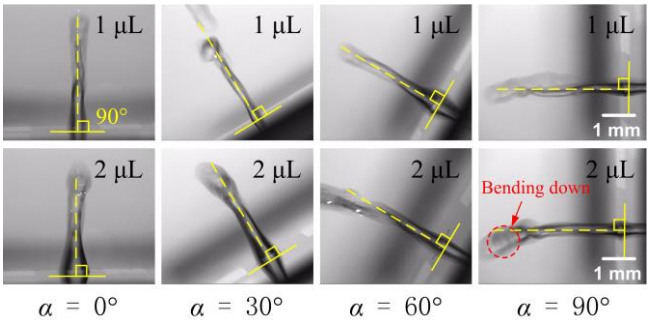

Fig. 9. Water droplet jetting images along inclined surfaces with inclination angles from 0° to 90° driven by standing waves with an input SAW power of 54 W.

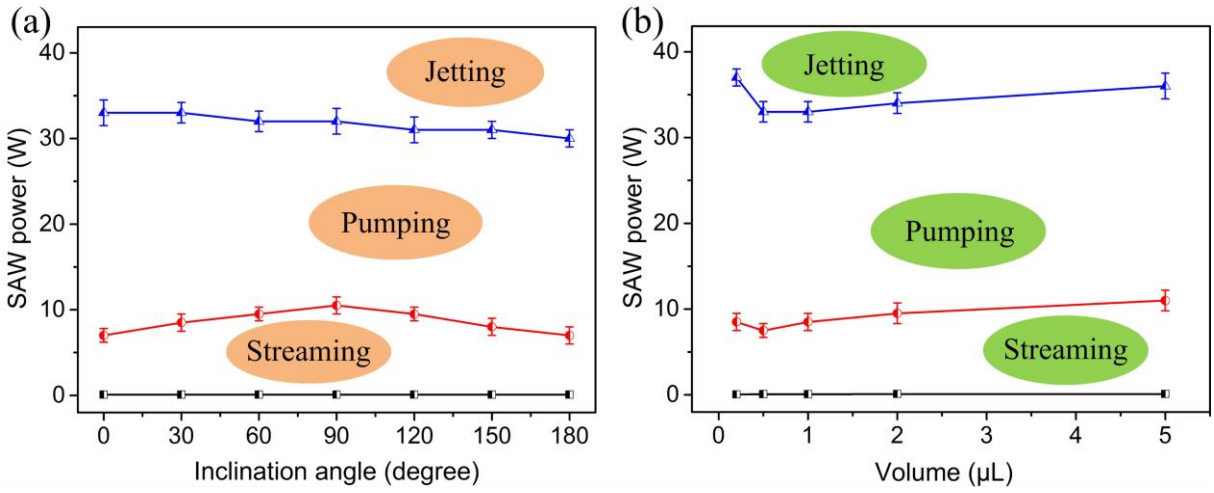

Fig. 10. (a) Summary of microfluidic power boundaries under different inclination angles and (b) power boundaries for different volume droplets at the inclination angle of 30°.

Fig. 10(a) summarizes microfluidic power boundaries for 1 μL droplet under different inclination angles. For AlN/Si SAW devices, acoustic streaming occurs at a lower RF power of a few mW. The threshold power to pump the droplet is about a few watts. As the inclination angle is increased from 0° to 90°, the threshold pumping power is increased and reaches its maximum value (10.5 W) at the inclination angle of 90°. The threshold pumping power is decreased with inclination angles increased from 90° to 180°. Higher RF power will result in the ejection of the droplet from the device surface and the minimum threshold jetting power (30 W) for 1 μL droplet occurs at the inclination angle of 180°. The power boundary values are comparable to those reported in previous studies [20, 21]. Fig. 10(b) shows power boundary values for different volume droplets at the inclination angle of 30°. As the droplet volume is increased from 0.5 μL to 5 μL, the threshold pumping power is increased. In addition, the jetting is slightly difficult for 0.2 μL droplet, probably due to smaller contact area between the device surface and the droplet, which could not provide enough concentrated SAW streaming force to eject the droplet.

4.3. Microfluidic performance comparisons between AlN/Si and ZnO/Si SAWs

A direct comparison of microfluidic performances between AlN/Si SAWs and ZnO/Si SAWs is difficult, as it is hard to obtain two types of films with identical properties. In order to compare their microfluidic performances as reasonable as possible, we fabricated a ZnO/Si SAW device with the same electrode configurations (wavelength, aperture and finger pairs) and almost same piezoelectric layer thickness (5 μm) as those of the AlN/Si SAW device. Table1 summarizes parameters and microfluidic performances between AlN/Si and ZnO/Si SAWs. We can see that ZnO/Si SAWs achieve lower threshold powers than those of AlN/Si SAWs. There are several factors which can cause this phenomenon.

Table 1. Comparisons of parameters and microfluidic performances between AlN/Si and ZnO/Si SAW devices.

Materials	ZnO/Si	AlN/Si
Wavelength (μm)	64	64
Piezoelectric film thickness (μm)	5	4.8
Resonant Frequency (MHz)	65.92	80.35
Electromechanical coupling coefficient k^2 (%)	1.06	0.25
Rayleigh angle (deg.)	20.8	16.9
SAW attenuation length (μm)	1013	717
Threshold pumping power (W)	3	8.5
Threshold jetting power (W)	12	33

Firstly, the electromechanical coupling coefficient k^2 of ZnO/Si SAW device is larger than that of AlN/Si SAW device, which means that when the same RF power is applied to the IDTs, ZnO/Si SAW device has a larger amplitude, thus generating larger SAW streaming force.

Secondly, the Rayleigh angle of ZnO/Si SAW device is larger than that of AlN/Si SAW device. The direction of SAW streaming force is following the Rayleigh angle. When the same SAW streaming force is applied onto the droplet, the larger the Rayleigh angle, the larger the component of acoustic streaming force along the surface. Fig. 11 shows the droplet deformation on 30° inclined surface driven by AlN/Si SAWs and ZnO/Si SAWs under their threshold pumping powers, respectively. The droplet lateral deformation along the inclined surface induced by ZnO/Si SAWs is slightly larger than that by AlN/Si SAWs due to their larger Rayleigh angles.

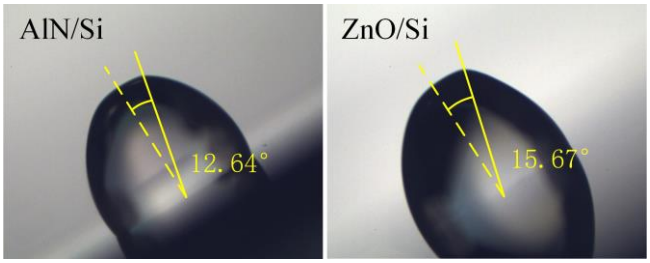

Fig. 11. The droplet deformation on 30° inclined surface driven by AlN/Si and ZnO/Si SAWs under their threshold pumping powers.

Thirdly, as ZnO films have lower acoustic velocity (~2700 m/s), the SAW attenuation length in liquid for ZnO film SAWs is larger than that for AlN film SAWs. The SAW attenuation length in liquids L_{SAW} can be estimated using [50]

$$L_{SAW} = \frac{\rho_s v_s \lambda}{\rho_f v_f} \tag{7}$$

where ρ_s is the substrate density, v_s is the SAW velocity in the substrate, λ is the device wavelength, ρ_f is the liquid density, and v_f is the sound velocity in the liquid. The SAW attenuation length reflects the interaction distance between the SAW and the droplet, a shorter SAW attenuation length will result in quicker dissipation of acoustic energy near the interaction point and consequently causes lesser energy dissipating into the droplet. Hence, for the same size droplet, the acting area of the SAW streaming force for ZnO/Si SAWs is larger than that for AlN/Si SAWs, and then resulting in lower threshold powers.

4.4. Acoustic heating performance comparisons between AlN/Si and ZnO/Si SAWs

When an RF power is applied to the IDTs, apart from the generated SAWs, there is also an acoustic heating effect. Recently, SAW heating effects have been used for microfluidic heating in lab-on-a-chip systems [51, 52]. However, most SAW heating devices are made on $LiNbO_3$ substrates, which are easily broken at a large thermal/electrical shock due to the brittle nature of the ceramic material. As opposed to $LiNbO_3$-based SAW devices, the cracking was seldomly observed in thin film SAW devices even they were driven at a high power of 60~70 W for a few minutes. The device breakdown is mainly from the damage of the contact pad or busbars of the IDTs when a high power is fed into the SAW device in an instant, which can be improved by increasing the size of the contact pad and width of busbars. Therefore, thin film SAWs have great potential for microfluidic heating applications.

Fig. 12(a) and (b) show acoustic heating performance comparisons between AlN/Si and ZnO/Si SAW devices. Results show that at the same input power, AlN/Si SAWs have higher surface temperature and quicker temperature response than those of ZnO/Si SAWs due to their lower electromechanical coupling coefficients and resulting in more applied powers transforming into the heat. Hence, AlN/Si SAWs have better acoustic heating performances than ZnO/Si SAWs. Besides, as shown in Fig. 12(c) and (d), the device heating temperatures can be digitally controlled by the input power and the SAW

heating shows good temperature stability and repeatability. Furthermore, in comparison with $LiNbO_3$ and ZnO films, AlN films have higher breakdown voltage and tolerating temperature (up to 700℃ in air), therefore AlN film SAWs are ideally suitable for microfluidic heating applications.

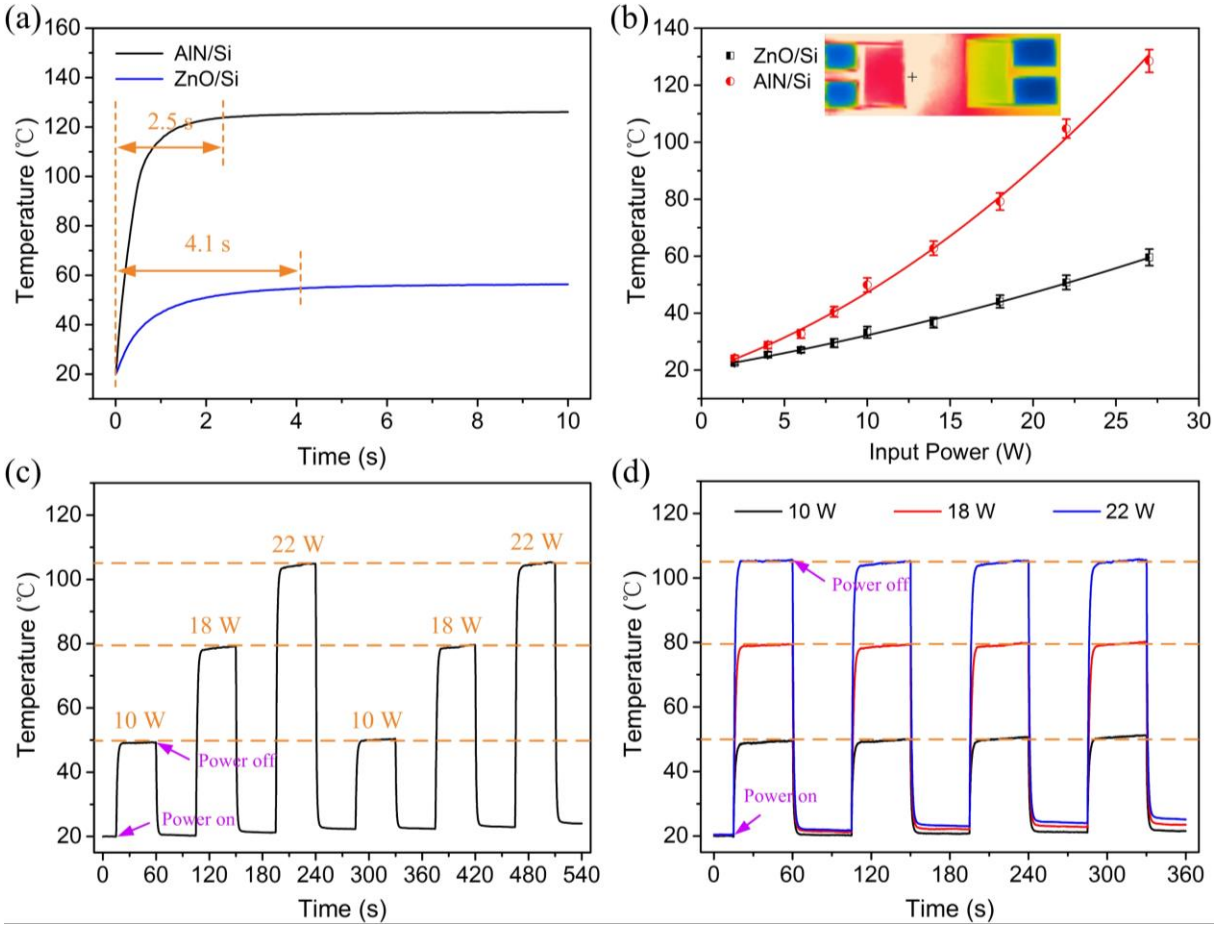

Fig. 12. (a) Surface temperatures for both AlN/Si and ZnO/Si SAW devices at the same point as a function of time with the same input power of 27 W, (b) surface temperatures of the SAW devices under different input SAW powers, the insert shows the heating image of the AlN/Si SAW device, (c) surface temperature changes of the AlN/Si SAW device under different power cycles, and (d) temperature stability and repeatability of the acoustic heating for AlN/Si SAW device.

The excessive SAW heating may have a negative effect on biological cells, thus limiting their use in certain biological applications. However, most biological applications using SAW technologies such as cell agglomeration, cellular spheroid assembly and enhancement of cell membrane penetrability are based on SAW streaming effect [53-55], which often occur at a lower power below 1 W, thereby resulting in an insignificant acoustic heating effect. Whereas, for some other applications such as the acceleration of biochemical reactions and polymerase chain reactions (PCRs) [52], AlN/Si SAW device will be a good choice. Therefore, AlN/Si SAW devices can be used for both actuators and acoustic heaters to achieve potential lab-on-a-chip applications.

5. Conclusions

AlN film-based SAW device was fabricated and characterized for acoustofluidic applications. Various microfluidic functions including transportation/pumping and jetting along inclined surfaces have been investigated. With the increased input SAW power or decreased droplet volume, the droplet pumping velocity is increased. A lower droplet pumping velocity and higher threshold pumping power were observed at 90° inclined surface due to the gravity effect. When the

droplet volume is small, for one-port propagating wave jetting, the jetting angles on the flat and inclined surfaces follow the Rayleigh angle. Whereas, for two-port standing wave jetting, the jetting angles on different inclined surfaces are vertical to the device surface and the maximum jetting height is increased with the input power or decreased droplet volume. Moreover, microfluidic and acoustic heating performances of the AlN/Si SAW device are further studied and compared with those of ZnO/Si SAW device with the same electrode configurations. Results show that ZnO/Si SAW device presents lower threshold powers, but AlN/Si SAW device has a more significant acoustic heating performance. Therefore, AlN film SAWs can not only be used for an actuator but also be used for a good acoustic heater to achieve potential lab-on-a-chip applications.

Acknowledgements

This work was supported by the "Zhejiang Provincial Natural Science Foundation of China (LZ19E050002)" and the "National Natural Science Foundation of China (51875521, 51605485 and 51575487)", Engineering Physics and Science Research Council of UK (EPSRC EP/P018998/1) and UK Fluidic Network-Special Interest Group of Acoustofluidics, and Newton Mobility Grant (IE161019) through Royal Society and NFSC.

References

[1] T. A. Franke, and A. Wixforth, "Microfluidics for miniaturized laboratories on a chip," *Chemphyschem*, vol. 9, no. 15, pp. 2140-2156, 2008.

[2] J. Friend, and L. Y. Yeo, "Microscale acoustofluidics: Microfluidics driven via acoustics and ultrasonics," *Rev. Mod. Phys.*, vol. 83, no. 2, pp. 647-704, 2011.

[3] L. Ren, Y. Chen, P. Li, Z. Mao, P. H. Huang, J. Rufo, F. Guo, L. Wang, J. P. McCoy, S. J. Levine, and T. J. Huang, "A high-throughput acoustic cell sorter," *Lab Chip*, vol. 15, no. 19, pp. 3870-3879, 2015.

[4] Y. Q. Fu, J. K. Luo, N. T. Nguyen, A. J. Walton, A. J. Flewitt, X. T. Zu, Y. Li, G. McHale, A. Matthews, E. Iborra, H. Du, and W. I. Milne, "Advances in piezoelectric thin films for acoustic biosensors, acoustofluidics and lab-on-chip applications," *Prog. Mater. Sci.*, vol. 89, pp. 31-91, 2017.

[5] M. Alghane, B. X. Chen, Y. Q. Fu, Y. Li, J. K. Luo, and A. J. Walton, "Experimental and numerical investigation of acoustic streaming excited by using a surface acoustic wave device on a 128° YX-LiNbO3 substrate," *J. Micromech. Microeng.*, vol. 21, no. 1, pp. 015005, 2010.

[6] M. Alghane, Y. Q. Fu, B. X. Chen, Y. Li, M. P. Y. Desmulliez, and A. J. Walton, "Streaming phenomena in microdroplets induced by Rayleigh surface acoustic wave," *J. Appl. Phys.*, vol. 109, no. 11, pp. 114901, 2011.

[7] R. Shilton, M. K. Tan, L. Y. Yeo, and J. R. Friend, "Particle concentration and mixing in microdrops driven by focused surface acoustic waves," *J. Appl. Phys.*, vol. 104, no. 1, pp. 014910, 2008.

[8] H. Ahmed, J. Park, G. Destgeer, M. Afzal, and H. J. Sung, "Surface acoustic wave-based micromixing enhancement using a single interdigital transducer," *Appl. Phys. Lett.*, vol. 114, no. 4, pp. 043702, 2019.

[9] L. Y. Yeo, and J. R. Friend, "Surface Acoustic Wave Microfluidics," *Annu. Rev. Fluid Mech.*, vol. 46, no. 1, pp. 379-406, 2014.

[10] A. Wixforth, "Acoustically driven planar microfluidics," *Superlattices Microstruct.*, vol. 33, no. 5, pp. 389-396, 2003.

[11] S. Collignon, J. R. Friend and L. Y. Yeo, "Planar microfluidic drop splitting and merging," *Lab Chip*, vol. 15, no. 8, pp. 1942-1951, 2015.

[12] Y. J. Guo, H. B. Lv, Y. F. Li, X. L. He, J. Zhou, J. K. Luo, X. T. Zu, A. J. Walton, and Y. Q. Fu, "High frequency microfluidic performance of LiNbO3 and ZnO surface acoustic wave devices," *J. Appl. Phys.*, vol. 116, no. 2, pp. 024501, 2014.

[13] C. Fu, A. J. Quan, J. T. Luo, H. F. Pang, Y. J. Guo, Q. Wu, W. P. Ng, X. T. Zu, and Y. Q. Fu, "Vertical jetting induced by shear horizontal leaky surface acoustic wave on 36° YX LiTaO3," *Appl. Phys. Lett.*, vol. 110, no. 17, pp. 173501, 2017.

[14] L. Y. Yeo, and J. R. Friend, "Ultrafast microfluidics using surface acoustic waves," *Biomicrofluidics*, vol. 3, no.1, pp. 012002-012002-23, 2009.

[15] K. Chono, N. Shimizu, Y. Matsui, J. Kondoh, and S. Shiokawa, "Development of novel atomization system based on SAW streaming," *Jpn. J. Appl. Phys.*, vol. 43, no. 5S, pp. 2987, 2004.

[16] J. Reboud, R. Wilson, Y. Zhang, M. H. Ismail, Y. Bourquin, and J. M. Cooper, "Nebulisation on a disposable array structured with phononic lattices," *Lab Chip*, vol. 12, no. 7, pp. 1268-1273, 2012.

[17] M. Wu, Z. Mao, K. Chen, H. Bachman, Y. Chen, J. Rufo, L. Ren, P. Li, L. Wang, and T. J. Huang, "Acoustic separation of nanoparticles in continuous flow," *Adv. Funct. Mater.*, vol. 27, no. 14, pp. 1606039, 2017.

[18] P. Li, Z. Mao, Z. Peng, L. Zhou, Y. Chen, P. H. Huang, C. I. Truica, J. J. Drabick, W. S. El-Deiry, M. Dao, and S. Suresh, "Acoustic separation of circulating tumor cells," *Proc. Natl. Acad. Sci.*, vol. 112, no. 16, pp. 4970-4975, 2015.

[19] J. Zhou, X. Tao, J. Luo, Y. Li, H. Jin, S. Dong, J. Luo, H. Duan, and Y. Fu, "Nebulization using ZnO/Si surface acoustic wave devices with focused interdigitated transducers," *Surf. Coat. Technol.*, vol. 367, no. 15, pp. 127-134, 2019.

[20] J. Zhou, M. DeMiguel-Ramos, L. Garcia-Gancedo, E. Iborra, J. Olivares, H. Jin, J. K. Luo, A. S. Elhady, S. R. Dong, D. M. Wang, and Y. Q. Fu, "Characterisation of aluminium nitride films and surface acoustic wave devices for microfluidic applications," *Sens. Actuator B: Chem.*, vol. 202, pp. 984-992, 2014.

[21] J. Zhou, H. F. Pang, L. Garcia-Gancedo, E. Iborra, M. Clement, M. D. Miguel-Ramos, H. Jin, J. K. Luo, S. Smith, S. R. Dong, D. M. Wang, and Y. Q. Fu, "Discrete microfluidics based on aluminum nitride surface acoustic wave devices," *Microfluid. Nanofluid.*, vol. 18, no. 4, pp. 537-548, 2015.

[22] Y. J. Guo, A. P. Dennison, Y. Li, J. Luo, X. T. Zu, C. L. Mackay, P. Langridge-Smith, A. J. Walton, and Y. Q. Fu, "Nebulization of water/glycerol droplets generated by ZnO/Si surface acoustic wave devices," *Microfluid. Nanofluid.*, vol. 19, no. 2, pp.273-282, 2015.

[23] Y. Li, Y. Q. Fu, S. D. Brodie, M. Alghane, and A. J. Walton, "Integrated microfluidics system using surface acoustic wave and electrowetting on dielectrics technology," *Biomicrofluidics*, vol. 6, no. 1, pp. 012812, 2012.

[24] Y. Wang, D. Chen, C. Wu, and J. Xie, "Effect of droplet boundary behaviors on SAW attenuation for potential microfluidic applications. *Jpn. J. Appl. Phys.*, vol. 58, no. 3, pp. 037001, 2019.

[25] J. Zhou, X. L. He, W. B. Wang, Q. Zhu, W. P. Xuan, H. Jin, S. R. Dong, M. D. Wang, and J. K. Luo, "Transparent surface acoustic wave devices on ZnO/glass using Al-doped ZnO as the electrode," *IEEE Electron Device Lett.*, vol. 34, no. 10, pp. 1319-1321, 2013.

[26] R. Tao, W. B. Wang, J. T. Luo, S. A. Hasan, H. Torun, P. Canyelles-Pericas, J. Zhou, W. P. Xuan, M. D. Cooke, D. Gibson, Y. Liu, Q. Wu, W. P. Ng, T. Franke, and Y. Q. Fu, "Thin film flexible/bendable acoustic wave devices: Evolution, hybridization and decoupling of multiple acoustic wave modes," *Surf. Coat. Technol.*, vol. 357, pp. 587-594, 2019.

[27] Y. Q. Fu, J. K. Luo, X. Y. Du, A. J. Flewitt, Y. Li, G. H. Markx, A. J. Walton, and W. I. Milne, "Recent developments on ZnO films for acoustic wave based bio-sensing and microfluidic applications: a review," *Sens. Actuator B: Chem.*, vol. 143, no. 2, pp. 606-619, 2010.

[28] X. Y. Du, Y. Q. Fu, J. K. Luo, A. J. Flewitt, and W. I. Milne, "Microfluidic pumps employing surface acoustic waves generated in ZnO thin films," *J. Appl. Phys.*, vol. 105, no. 2, pp. 024508, 2009.

[29] Y. Q. Fu, Y. Li, C. Zhao, F. Placido, and A. J. Walton, "Surface acoustic wave nebulization on nanocrystalline ZnO film," *Appl. Phys. Lett.*, 101(19), p.194101, 2012.

[30] Y.Q. Fu, L. Garcia-Gancedo, H. F. Pang, S. Porro, Y. W. Gu, J. K. Luo, X. T. Zu, F. Placido, J. I. B. Wilson, A. J. Flewitt, and W. I. Milne, "Microfluidics based on ZnO/nanocrystalline diamond surface acoustic wave devices," Biomicrofluidics, vol. 6, no. 2, pp. 024105, 2012.

[31] I. H. Kim, D. Y. Ku, J. H. Ko, D. Kim, K. S. Lee, J. H. Jeong, T. S. Lee, B. Cheong, Y. J. Baik, and W. M. Kim, "Improvement of the thermal and chemical stability of Al doped ZnO films," *J. Electroceram.*, vol. 17, no. 2, pp. 241-245, 2006.

[32] H. Cheng, Y. Sun, Y. B. Zhang, J. X. Zhang, S. Yuan, and P. Hing, "AlN films deposited under various nitrogen concentrations by RF reactive sputtering," *J. Cryst. Growth*, vol. 254, no. 1, pp. 46-54, 2003.

[33] G. F. Iriarte, J. G. Rodríguez, and F. Calle, "Synthesis of c-axis oriented AlN thin films on different substrates: A review," *Mater. Res. Bull.*, vol. 45, no. 9, pp. 1039-1045, 2010.

[34] Y. Wang, Z. Xu, Y. Wang, and J. Xie, "A study on AIN film-based SAW attenuation in liquids and their potential as liquid ethanol sensors," *Sensors*, vol. 17, no. 8, pp. 1813, 2017.

[35] Y. Wang, D. Chen, X. Chen, D. Li, C. Wu, and J. Xie, "A surface acoustic wave device for water impurity levels monitoring by measuring signal-to-perturbation ratios," *Jpn. J. Appl. Phys.*, vol. 58, no. 6, pp. 061002, 2019.

[36] Y. Wang, Y. Wang, W. Liu, D. Chen, C. Wu, and J. Xie, "An aerosol sensor for PM1 concentration detection based on 3D printed virtual impactor and SAW sensor," *Sens. Actuators A: Phys.*, vol. 288, pp. 67-74, 2019.

[37] A. Bussonnière, M. Baudoin, P. Brunet, and O. B. Matar, "Dynamics of sessile and pendant drops excited by surface acoustic waves: Gravity effects and correlation between oscillatory and translational motions," *Phys. Rev. E*, vol. 93, no. 5, pp. 053106, 2016.

[38] M. Abdelgawad, S. L. Freire, H. Yang, and A. R. Wheeler, "All-terrain droplet actuation," *Lab Chip*, vol. 8, no. 5, pp. 672-677, 2008.

[39] E. De Jong, Y. Wang, J. M. Den Toonder, and P. R. Onck, "Climbing droplets driven by mechanowetting on transverse waves," *Sci. Adv.*, vol. 5, no. 6, pp. eaaw0914, 2019.

[40] S. Datta, A. K. Das, and P. K. Das, "Uphill movement of sessile droplets by electrostatic actuation," *Langmuir*, vol. 31, no. 37, pp. 10190-10197, 2015.

[41] S. Datta, M. Sharma, and A. K. Das, "Investigation of upward climbing motion of a droplet over an inclined surface using electrowetting," *Ind. Eng. Chem. Res.*, vol. 53, no. 16, pp. 6685-6693, 2014.

[42] N. Janardan, and M. V. Panchagnula, "Effect of the initial conditions on the onset of motion in sessile drops on tilted plates," *Colloid Surf. A-Physicochem. Eng. Asp.*, vol. 456, no. 1, pp. 238-245, 2014.

[43] B. Krasovitski, and A. Marmur, "Drops down the hill: Theoretical study of limiting contact angles and the hysteresis range on a tilted plate," *Langmuir*, vol. 21, no. 9, pp. 3881-3885, 2005.

[44] A. I. ElSherbini, and A. M. Jacobi, "Liquid drops on vertical and inclined surfaces: I. An experimental study of drop geometry," *J. Colloid Interf. Sci.*, vol. 273, no. 2, pp. 556-565, 2004.

[45] W. L. M. Nyborg, "Acoustic Streaming," in *Physical Acoustics*, edited by e. W. P Mason (Academic, New York, USA, 1965), pp. 265-331.

[46] S. Shiokawa, Y. Matsui, and T. Ueda, "Study on SAW streaming and its application to fluid devices," *Jpn. J. Appl. Phys.*, vol. 29, no. S1, pp. 137-139, 1990.

[47] B. S. Yilbas, A. Al-Sharafi, H. Ali, and N. Al-Aqeeli, "Dynamics of a water droplet on a hydrophobic inclined surface: influence of droplet size and surface inclination angle on droplet rolling," *RSC Adv.*, vol. 7, no. 77, pp. 48806-48818, 2017.

[48] C. G. L. Furmidge, "Studies at phase interfaces. I. The sliding of liquid drops on solid surfaces and a theory for spray retention," *J. Colloid Sci.*, vol. 17, no. 4, pp. 309-324, 1962.

[49] P. Tsai, R. G. Lammertink, M. Wessling, and D. Lohse, "Evaporation-triggered wetting transition for water droplets upon hydrophobic microstructures," *Phys. Rev. Lett.*, vol. 104, no. 11, pp.116102, 2010.

[50] L. Schmid, A. Wixforth, D. A. Weitz, and T. Franke, "Novel surface acoustic wave (SAW)-driven closed PDMS flow chamber," *Microfluid. Nanofluid.*, vol. 12, no. 1-4, pp. 229-235, 2012.

[51] K. Kulkarni, J. Friend, L. Yeo, and P. Perlmutter, "Surface acoustic waves as an energy source for drop scale synthetic chemistry," *Lab Chip*, vol. 9, no. 6, pp. 754-755, 2009.

[52] J. Reboud, Y. Bourquin, R. Wilson, G. S. Pall, M. Jiwaji, A. R. Pitt, A. Graham, A. P. Waters, and J. M. Cooper, "Shaping acoustic fields as a toolset for microfluidic manipulations in diagnostic technologies," *Proc. Natl. Acad. Sci.*, vol. 109, no. 38, pp. 15162-15167, 2012.

[53] Y. Kurashina, K. Takemura, and J. Friend, "Cell agglomeration in the wells of a 24-well plate using acoustic streaming," *Lab Chip*, vol. 17, no. 5, pp. 876-886, 2017.

[54] L. Alhasan, A. Qi, A. Al-Abboodi, A. Rezk, P. P. Chan, C. Iliescu, and L. Y. Yeo, "Rapid enhancement of cellular spheroid assembly by acoustically driven microcentrifugation," *ACS Biomater. Sci. Eng.*, vol. 2, no. 6, pp. 1013-1022, 2016.

[55] H. Li, J. Friend, L. Yeo, A. Dasvarma, and K. Traianedes, "Effect of surface acoustic waves on the viability, proliferation and differentiation of primary osteoblast-like cells," *Biomicrofluidics*, vol. 3, no. 3, pp. 034102, 2009.